JOURNAL OF GEOPHYSICAL RESEARCH, VOL. ???, XXXX, DOI:10.1029/,

Regional P-wave Velocity Structure of the Northern Cascadia Subduction Zone

K. Ramachandran[1,2], R. D. Hyndman[1], and T. M. Brocher[3]

K. Ramachandran, Department of Geological Sciences and Geological Engineering, Queen's University, Kingston, Ontario K7L3N6, Canada. (ramachandran@geol.queensu.ca)

R. D. Hyndman, Pacific Geoscience Centre, Geological Survey of Canada, 9860 W Saanich Road, Sidney, B.C. V8L 4B2, Canada. (hyndman@pgc.nrcan.gc.ca)

T. M. Brocher, U.S. Geological Survey, MS 977, 345 Middlefield Road, Menlo Park, CA 94025 USA. (brocher@usgs.gov)

[1]Geological Survey of Canada, Sidney, B.C., Canada

[2]Now at Queen's University, Kingston, Ontario, Canada

[3]U.S. Geological Survey, Menlo Park, CA, USA

Abstract.

This paper presents the first regional three dimensional P-wave velocity model for the Northern Cascadia Subduction Zone (S.W. British Columbia and N.W. Washington State) constructed through tomographic inversion of first-arrival times from active source experiments together with earthquake travel-time data recorded at permanent stations. The velocity model images the structure of the subducting Juan de Fuca plate, megathrust, and the fore-arc crust and mantle. Beneath southern Vancouver Island, the megathrust above the Juan de Fuca plate is characterized by a broad zone (25–35 km depth) having relatively low velocities of 6.4–6.6 km/s. These low velocities are inferred to represent subducting sedimentary rocks of the accretionary wedge. This relative low velocity zone coincides with the location of most of the episodic tremors recently mapped beneath Vancouver Island and its low velocity may also partially reflect the presence of trapped fluids and sheared lower crustal rocks. Serpentinization of the upper forearc mantle provides evidence for slab dewatering and densification. Tertiary sedimentary basins in the Strait of Georgia and Puget Lowland imaged by the velocity model lie above the inferred region of slab dewatering and densification and may therefore partly result from a higher rate of slab sinking. In contrast, sedimentary basins in the Strait of Juan de Fuca lie in a synclinal depression in the Crescent Terrane. The correlation of inslab earthquake hypocenters $\mathbf{M} > 4$ with P-wave velocities greater than 7.8 km/s suggest that they orig-

inate near and possibly below the oceanic Moho of the subducting Juan de Fuca plate.

1. Introduction

Northern Cascadia subduction zone in the Pacific Northwest of North America is a region of high earthquake hazard. Megathrust earthquakes, such as the one that occurred in 1700 [*Satake et al.*, 1996], have an average recurrence of ∼500 to 600 years [*Atwater and Hemphill-Halley*, 1997] and nearly 10 earthquakes of magnitude 6 and above have occurred in the past 125 years [e.g., *Clague*, 1997]. Cenozoic forearc basins such as the Seattle, Tacoma, and the Georgia basins may amplify ground motion due to earthquake energy in high population centers [e.g., *Pratt et al.*, 2003]. An accurate estimate of the subsurface velocity structure is necessary to model the shaking effects of earthquakes and to relocate earthquakes. The main objective of this study is to construct a large scale P-wave velocity model for the northern Cascadia subduction zone through tomographic inversion of active source and earthquake data from S.W. British Columbia, Canada and N.W. Washington State, USA (Figure 1).

The tomographic inversion included 147,000 first arrival times recorded at 225 temporary stations widely distributed over S.W. British Columbia and N.W. Washington from the Seismic Hazards Investigation in Puget Sound (SHIPS) experiment in 1998 [*Fisher et al.*, 1999; *Brocher et al.*, 1999]. In addition, 72,000 arrival times from approximately 3,000 local earthquakes recorded at 91 permanent recording stations located in S.W. British Columbia and N.W. Washington were also employed in the inversion. The minimum structure velocity model constructed in this study provides the first regional image of the the northern Cascadia subduction zone obtained from a single tomographic inversion. The velocity model helps constrain the position of the subducting plate along a

300 km north-south stretch of the northern Cascadia subduction zone representing nearly one-fourth of the entire zone. The relocated inslab earthquake positions and the associated velocity at the hypocenters provide evidence that the inslab earthquakes occur very close to, and possibly below, the base of the subducting crust.

2. Geology, Tectonics, and Seismicity

The Intermontane superterrane (Figure 1, top right inset), made up mostly of sedimentary and volcanic rocks, collided with the North America plate, about 200 My ago. The last major collisional episode around mid-Cretaceous time, emplaced the Insular superterrane against the Intermontane superterrane, and generated the mid-Cretaceous to early Tertiary intrusive rocks of the Coast Belt in the suture region [*Monger et al.*, 1982; *Monger*, 1990] (Figure 2). The two superterranes underlie the Intermontane and Insular belts, respectively (Figure 2). In the S.W. British Columbia margin, Vancouver Island is dominated by Wrangellia terrane, emplaced during the middle Cretaceous [*Smith and Tipper*, 1986], thought to represent a largely Jurassic island arc [*Jones et al.*, 1977; *Muller*, 1977]. The mainly meta-sedimentary Mesozoic Pacific Rim terrane and the volcanic Eocene Crescent Terrane lie along the west coast and southern end of Vancouver Island and were the last to accrete to the continent and reached their present locations during late Cretaceous and Tertiary periods [*Johnson*, 1984]. To the south of Vancouver Island, the Strait of Juan de Fuca lies in the synclinal depression formed in the Crescent Terrane. To the east of Vancouver Island, the Strait of Georgia is a forearc basin that straddles the boundary of the Insular and Coast belts.

The N.W. Washington margin is comprised of the Coast Range province to the west and the Cascade Range province to the east (Figure 2). The Coast Range province includes the

Olympic Subduction Complex and Puget Sound. To the east of the Olympic Subduction Complex, the Puget Sound is a forearc basin. The Cascade Range province to the east of Puget Lowland comprises of a variety of igneous, sedimentary and metamorphic rocks that comprise several distinct crustal terranes [e.g., *Tabor*, 1994].

The Juan de Fuca oceanic plate converges with the North America continental plate at a relative rate of ∼46 mm/a directed N56°E [*Riddihough and Hyndman*, 1991]. Subduction of the Juan de Fuca plate has resulted in a number of damaging earthquakes [e.g., *Rogers, 1998*]. Earthquakes occur in three distinctive source regions, a) earthquakes in the North American continental crust, b) earthquakes in the subducting oceanic plate and c) megathrust earthquakes at the interface of the oceanic and the North American plates. The relatively large number of earthquakes in the continental crust are driven by a north-northwest compressive stress parallel to the continental margin [e.g., *Rogers*, 1998]. The deeper earthquakes, in the depth range of 40–70 km, occur due to a tensional stress regime within the subducted oceanic plate. Paleoseismic evidence shows that megathrust earthquakes have occurred at intervals of 500–600 years [*Atwater and Hemphill-Halley*, 1997]; latest occurred in 1700 [*Satake et al.*, 1996].

3. Data

Data from active source experiments and earthquake recordings were used to construct a three-dimensional P-wave minimum structure velocity model. The active source data constrains the upper crustal velocities that have large lateral variations between the sedimentary basins and the basement rocks made up of accreted terranes. The well-constrained upper crustal velocity structure improves the estimation of deeper velocities and earthquake hypocentral parameters.

3.1. Active Source Data

The 1998 SHIPS experiment [*Fisher et al.*, 1999; *Brocher et al.*, 1999] recorded arrivals from a total of 33,000 air-gun shots fired on 11 shot lines in the waterways of the Strait of Georgia, the Strait of Juan de Fuca, and Puget Sound (Figure 1). The shots were recorded widely over southwestern British Columbia and northwestern Washington (Figure 1) at 257 temporary land-based, Reftek stations [*PASSCAL*, 1991], and 15 ocean-bottom seismometers at offsets from 1 to 370 km [*Brocher et al.*, 1999]. Approximately 147,000 first arrival time picks from 225 temporary recording stations were employed in the inversion. In addition, 1000 first arrival travel times from a refraction line acquired in 1991 [*Miller et al.*, 1997] were also included.

3.2. Earthquake Data

Approximately 70,000 first arrival times from nearly 3000 earthquakes that occurred in the S.W. British Columbia and N.W. Washington margin, recorded at 91 permanent recording stations (Figure 1, left bottom inset) in the past 25 years were used in the tomographic inversion. Selection criteria included earthquakes from all depths, which were recorded by at least six stations within the study region. Hypocentral data from the earthquake catalogs were used as the initial hypocentral parameters for the tomographic inversion.

4. Tomographic Inversion

The tomographic inversion method is based on iterative linearized inversion of the travel-time equations, regularized by minimizing the vertical and horizontal roughness of the model subject to the constraint of fitting the travel-time data to within estimated obser-

vational uncertainties using the χ^2 criterion [e.g. *Zelt and Barton*, 1998]. The noise present in the data is assumed to be Gaussian, in which case the acceptable data misfit is set to the expected value for the normalized χ^2 misfit statistic, *i.e.* $\Delta t^T \mathbf{C}_d^{-1} \Delta t/(N-1) = 1$, where Δt is the travel-time data residual vector; $\mathbf{C}_d$ is a diagonal matrix representing the variance of the travel-time measurements; N is the number of data. Further details about the methodology employed for joint inversion of earthquake and active source data can be found in *Ramachandran* [2001] and *Ramachandran et al.* [2005].

The velocity model was parameterized in the forward and inverse steps by a node and cell spacing of (1.5 × 1.5 × 1.5) km and (4.5 × 4.5 × 1.5) km, respectively. The velocity model dimensions in (x, y, z) directions are (460 × 490 × 96) km. The top of the model is set to 3 km above sea-level to allow positioning the receivers at their actual elevations in the velocity model. An initial 1-D velocity model consistent with the regional geology was constructed by forward modeling the travel time data. The travel-time misfit for the initial model as a function of offset for the SHIPS data and the earthquake events is shown in Figures 3a and 3c, respectively. The RMS travel-time residual for this model for approximately 210,000 observations was 762 ms for a normalized χ^2 of 52. During the tomographic inversion, the hypocentral parameters and the velocity model were updated after each iteration. Ray tracing was performed during each iteration to account for the change in the hypocentral parameters between iterations. After 30 iterations, a stable minima was obtained at an RMS misfit of ∼132 ms and normalized χ^2 of ∼1.1, which represents a 97% variance reduction. The travel-time misfit with offset for the final model for the SHIPS data and the earthquake events is shown in Figures 3b and 3d, respectively.

4.1. Ray Hit Count and Checkerboard Tests

The ray hit count method offers a quick and easy way to assess the velocity constraint for each cell. Rays were traced though the final velocity model with the actual receiver geometry, relocated earthquake positions, and active source positions to determine the number of rays that pass through each cell. The ray hit counts for 3–27 km and 21–57 km depth range are shown in Figure 4a and 5a, respectively. The results show significant ray coverage in the upper and middle crust down to 20 km where most of the rays are from the SHIPS active source data set. The ray coverage in the mid crust and below are primarily from the earthquake data and is sparser. However, since these rays from deeper earthquakes travel through the well constrained upper crustal velocity model, the velocities modeled for the lower crust and upper mantle are inferred to be well constrained.

Checkerboard tests were carried out with grid sizes of 30, 40 and 50 km to access the ability of the data to resolve model features of these sizes at different depth levels. Semblance values measuring the correlation between the input and recovered patterns, as discussed by *Zelt and Barton* [1998], were used to classify model volumes having reasonable lateral resolution. Semblance values of 1 and 0.5 indicate total recovery of the velocity perturbation and no recovery of the velocity perturbation, respectively. Semblance values less than 0.5 indicate negative correlation. Semblance values between the initial and recovered checkerboard anomaly patterns were computed with a window size of 16.5×16.5×3.0 km.

The recovered checkerboard anomaly pattern for a grid size of 30 km between depths of 0–21 km (Figure 4b) is characterized by semblance values of 0.7 and above (Figure 4c), indicating adequate resolution. The sedimentary basins in the Straits of Georgia and

Juan de Fuca, and the Puget Lowland show good recovery of the checkerboard anomaly patterns in the depth slices at 3 and 9 km. The low semblance values on the fringe of the model (Figure 4c) are inferred to be due to limited ray directivity and fewer rays at the edges. The recovered checkerboard anomaly pattern and semblance values for a grid size of 40 km indicate adequate resolution down to 45 km depth for features of this size. The recovered checkerboard anomaly pattern for a grid size of 50 km (Figure 5b), between 21 to 57 km depth suggests that the ray coverage is sufficient to recover features of this size. Semblance plots (Figure 5c) indicate adequate lateral resolution at all depth levels west of 122.25° W. East of 122.25° W, average resolution is inferred at depths between 45 and 57 km .

5. Results & Discussion

Vertical cross-sections along selected orientations (Figures 6, 7, & 8) and horizontal (depth) slices (Figure 9) define the structure of the subducting Juan de Fuca plate. A horizontal velocity slice at 3 km depth along with the inferred outline of the younger sedimentary basins (Figure 10a) and a gravity anomaly map of the region (Figure 10b) present the sedimentary basins setting in relation to the forearc mantle wedge.

5.1. Lower crustal low velocity zone

A broad zone of low velocities is imaged in the lower crust, between 25 and 35 km depth, beneath Vancouver Island on the vertical cross-sections AB, CD, EF, PQR and MNO (Figures 6 and 8). The lateral extent of the low velocity zone above the subducting plate is seen in the horizontal velocity slices at 27 and 33 km (Figure 9a and 9b). *Cassidy*

and Ellis [1991] identified a crustal low velocity zone between 20–26 km depth at station *ALB* (Figure 6a) from receiver function studies.

This broad low velocity zone in the lower crust correlates with an approximately 5–8 km thick band of reflectivity in the lower crust beneath Vancouver Island identified from the 1984 Vancouver Island LITHOPROBE Vibroseis reflection lines [*Clowes et al.*, 1987]. This band of reflective zone is generally referred to as E reflectivity. *Hyndman* [1988] suggested that fluids released from the dehydration reactions occurring in the subducting slab can be trapped at this depth level and account for the seismic E reflectors. *Calvert and Clowes* [1990] suggested a shearing mechanism for these reflectors.

Earthquake locations do not fall within this low velocity zone (Figures 6 and 8) and it is inferred that any accumulated stress there is probably released by episodic, aseismic slow slip events [*Dragert et al.*, 2001]. *Rogers and Dragert* [2003] identified non-earthquake tremor-like signals accompanying the episodic aseismic slip. The episodic tremors distribute over a wide depth range of $\sim$40 km, with a peak at 25–35 km and many of these events occur within or in the close vicinity to the E reflectors [*Kao et al.*, 2005]. Approximately 50% of the episodic tremor events are located within or close to the E reflectors [*Kao et al.*, 2005], whereas $> 90\%$ of the local earthquakes tend to be located away from the reflectors [*Calvert*, 2004]. *Kao et al.* [2005] suggest that shear deformation and fluids may be closely related to the occurrence of episodic tremor. The low velocities imaged between 25–35 km depth beneath Vancouver Island coincides with the zone of postulated mechanisms of shearing and presence of fluids inferred from EM measurements [*Hyndman*, 1988].

5.2. Olympic Subduction Complex

Eocene and younger clastic sedimentary rocks scraped off the subducting Juan de Fuca plate are accreted to North America as a thick accretionary prism along the Cascadia subduction zone margin, mainly beneath the shelf and the continental slope [*Tabor and Cady*, 1978]. The accretionary prism has been uplifted, metamorphosed and exposed in the Olympic Peninsula [e.g., *Brandon and Calderwood*, 1990] (Figure 2). The low velocity rocks of the Olympic Subduction Complex exhibit a sharp velocity contrast with the neighboring and overlying Crescent terrane rocks as can be clearly observed on cross-sections GH and IJ (Figure 7). A similar velocity contrast is also seen in laboratory studies; the Crescent terrane volcanic rocks exhibit a velocity contrast of up to 1.0 km/s with the low velocity Core rocks from the Olympic Peninsula [*Brocher and Christensen*, 2001]. From the cross sections GH, IJ, and KL (Figure 7) we infer that the low velocity rocks of the Olympic Subduction Complex underthrust the Crescent terrane and extend to at least 30 km depth. The Olympic Core rocks appear to extend downward to the top of the Juan de Fuca plate.

The eastward underthrusting of the low velocity rocks of the Olympic Subduction Complex deform the overlying Crescent Terrane and is probably the source of some seismicity in the depth range of 15 to 30 km (Figure 7b, model distance 50–100 km; figure 8a, Line QR model distance 20–130 km). However, earthquake mechanisms in the forearc [e.g., *Wang et al.*, 1995] and GPS data [e.g., *Hyndman et al.*, 2003] indicate northward compression of the forearc against the British Columbia buttress as the main source for the earthquakes in this region. The low velocity rocks of the Olympic Subduction Com-

plex themselves are inferred from our study to be aseismic as evidenced by the lack of earthquakes within the low velocity rocks.

5.3. Location of the Forearc Basins and Slab dehydration

Locations of sedimentary basins outlined as velocity anomaly lows in the horizontal velocity slice at 3 km depth (Figure 10a) and as gravity anomaly lows (Figure 10b) show a strong correlation. The sedimentary basins are classified into two groups (Figure 10b); several larger basins in the Strait of Georgia and the Puget Sound, and several smaller basins in the Strait of Juan de Fuca. The sedimentary basins in the Strait of Georgia and the Strait of Juan de Fuca were previously detailed from 3-D tomographic P-wave velocity models by *Zelt et al.* [2001] and *Ramachandran et al.* [2004]. *Brocher et al.* [2001], *Tréhu et al.* [2002], and *Van Wagoner et al.* [2002] mapped the locations of the sedimentary basins in Puget Sound from 3-D velocity models. The velocity model from the present study provides the first contiguous image of all the sedimentary basins in the Strait of Georgia, the Strait of Juan de Fuca, and the Puget Lowland (Figure 10a).

The thick red dashed line shown in Figure 10b marks the approximate position of the junction of the subducting Juan de Fuca crust and the forearc mantle wedge. East of this boundary, the basins in the Strait of Georgia and Puget Sound lie above the zone of inferred forearc mantle serpentinization. Dehydration, eclogitization, and densification of the slab crust [*Peacock*, 1993] and slab mantle dehydration and densification [e.g., *Hacker et al.*, 2003] decrease the buoyancy of the oceanic plate with respect to the surrounding mantle [*Rogers*, 1983]. This phase change may be reflected as a small increase in the angle of subduction of young plates in the subduction zones of Cascadia, southern Chile, and the Nankai region of SW Japan [e.g. *Rogers*, [2002]. The change of subduction angle at

such a shallow depth may foster forearc basin subsidence. Sub-crustal erosion and cooling of the forearc continental crust may also contribute to forearc basin subsidence.

In contrast to the larger basins in the Strait of Georgia and Puget Sound, the small Clallam and Sequim basins in the Strait of Juan de Fuca lie in the synclinal depression formed in the Crescent Terrane. The synclinal depression was probably formed in the Crescent Terrane due to folding and faulting in the Strait of Juan de Fuca and Olympic Peninsula to accommodate the northward motion of the Coast Range block along the Coast Range Boundary Fault [*Snavely*, 1987].

5.4. Juan de Fuca Plate Position

Our P-wave velocity model is a significant improvement over previous velocity models because of the inclusion of a large set of earthquake picks from a broader distribution of permanent stations and a denser distribution of active source travel-times. The velocity model images oceanic mantle rocks which are inferred to have velocities greater than $\sim$7.6 km/s. This isocontour is assumed to define the top of the oceanic Moho. The top of the Juan de Fuca crust is drawn as a smooth surface approximately 7 km above the oceanic Moho, assuming an average oceanic crustal thickness. Using these constraints, the interpreted position of the top of the Juan de Fuca crust and mantle are shown on the cross sections in Figures 6, 7 & 8.

Estimates of crustal thickness and slab geometry from Figures 6, 7, & 8 match those of several previous workers, including *Hyndman et al.* [1990]'s interpretation that a short reflection segment at 10 s two-way time on LITHOPROBE line 84-01, referred to as the F reflection, represents the top of the Juan de Fuca crust. Our estimate for the depth to the oceanic crust agrees with that suggested by *Drew and Clowes* [1990] from

refraction data modeling. These depth estimates were also substantiated by *Tréhu et al.* [2002] and *Calvert* [2004] through analysis of reflection and refraction seismic data from Vancouver Island and adjoining waterways. Our estimates are also consistent with the depth estimates derived from receiver function analysis of *Cassidy and Ellis* [1993] and *Cassidy* [1995].

The agreement, however, is not universal. *Nedimović et al.* [2003] suggested that the position of the Juan de Fuca crust is geometrically below the E reflectors and is shallower than previous estimates by at least 6 km beneath Vancouver Island. If the depth to the top of the crust is brought shallower by 6 km, as suggested by *Nedimović et al.* [2003], the oceanic mantle would be represented by velocities in the range of ∼7.2 km in our velocity model, which then would be indicative of extensive serpentinization of the oceanic mantle rocks. At this time, there is not enough evidence to suggest extensive oceanic mantle sepentinization in this region to account for a oceanic mantle velocity of ∼7.2 km.

Through the analysis of P coda from teleseismic events, *Nicholson et al.* [2005] interpreted the position of the Juan de Fuca crust to coincide with the E reflection zone. Their estimates for the depth to the top of the Juan de Fuca crust beneath Vancouver Island are shallower than previous estimates by at least 10 km. It is increasingly difficult to correlate our velocity model with the position of the Juan de Fuca plate suggested by *Nicholson et al.* [2005] for the same reasons discussed for the model of *Nedimović et al.* [2003].

5.5. Juan de Fuca Plate Seismicity

It is previously suggested that oceanic slab earthquakes at depths below ∼35 km are induced by dehydration-embrittlement processes in the slab crust [e.g., *Kirby et al.*, 1996]

and in the slab mantle [e.g., *Peacock*, 2001; *Hacker et al.*, 2003]. On the vertical cross-sections (Figures 6 & 7), the earthquakes occurring in the region with velocities in the range of 7.6–8.0 km/s are inferred to occur in the slab mantle. From relocated slab earthquakes beneath the Strait of Georgia, *Cassidy and Waldhauser* [2003] demonstrated that some of the slab earthquakes originated in the oceanic mantle. Beneath the Olympic Peninsula and Puget Sound, significant number of inslab earthquakes lie in regions with velocities between 7.6 and 8.0 km/s [*Preston et al.*, 2003, Supplemental online material, Table S1]. Almost fully eclogitized slab crust and weakly serpentinized upper mantle are expected to be in this velocity range.

Peacock [2001] proposed that sea water percolating along fault zones at the outer rise could hydrate and serpentinize the slab's upper mantle. This process may reduce the velocity of the oceanic mantle below the normal ∼8.2 km/s on Figures 7, 8 and 9. As observed on the horizontal slice at 45 and 51 km depth (Figure 6, 7, & 8; Figure 9d & e), the levels of seismicity inferred in the slab mantle beneath the Washington margin are higher than along the British Columbia margin. This increase may reflect higher levels of oceanic mantle de-serpentinization and fluid expulsion beneath the Washington margin, facilitating seismic rupture.

The distribution of earthquakes used in this study (Figure 1, bottom left inset) is representative of the occurrence of earthquakes in the forearc upper crust and the Juan de Fuca slab [e.g., *McCrory et al.*, 2004]. The inslab earthquakes occurring below 35 km depth and inferred to be within the Juan de Fuca slab are summarized in Table 1 by depth range. The earthquakes within a depth range are classified into three different groups according to the P-wave velocity at their hypocenter: 6.8–7.2 km/s (slab upper crust with

hydrous minerals), 7.2–7.8 km/s (mid to lower slab crust and partially eclogitized slab upper crust and serpentinized upper mantle), and 7.8–8.2 km/s (slab mantle that may be partially serpentinized).

The crust and uppermost mantle of warm slabs dehydrate at shallow depths [e.g., *Hacker et al.,* 2003; *Peacock and Wang*, 1999; *Currie et al.*, 2002]. Thermal modeling for warm slabs like Juan de Fuca show that metamorphic reactions in the subducting oceanic crust can start as shallow as 40–50 km depth [*Peacock et al.*, 2002]. Depending on the amount mantle serpentinization, the hypocentral regions of inslab earthquakes in the subducting mantle will have a velocity of 7.8–8.2 km/s. In contrast, the hypocentral regions of shallow earthquakes in the slab crust are expected to have a seismic velocity range of 6.8–7.2 km/s. Between 35–40 km depth in Table 2, the number of hypocentral regions having velocities between 6.8 and 7.2 km/s is lower than the number of hypocentral regions having velocities between 7.2 and 7.8 km/s. This finding suggests that more earthquakes occur in the slab's partially eclogitized crust than in unaltered crust. Hypocentral regions having velocities between 7.8 and 8.2 km/s velocity zone are inferred to occur within the slab's nearly fully eclogitized crust and/or partly serpentinized slab mantle. Between 40 and 50 km depths, significantly larger number of hypocenters occur in the region having a velocity range between 7.8 and 8.0 km/s (Table 2). This result suggests that these earthquakes occur close to the slab Moho. At 50–60 km depth interval, hypocenters in the 7.8–8.2 km/s velocity zone dominate the distribution, and below 60 km depth no hypocenters are observed in the velocity range of 6.8–7.8 km/s. Hence, it is inferred that the earthquakes in the slab between 50 and 60 km depth occur in the nearly fully eclogitized oceanic crust and/or the oceanic upper mantle.

Our results indicate that most inslab earthquakes originate close to the slab Moho. *Cassidy and Waldhauser* [2003] showed that the large events do occur in the uppermost mantle, and there is little activity in the lower slab crust. *Wada et al.* [2004] showed that many events along the Nankai margin, SW Japan occur in the slab mantle. The recent, warm slab, damaging earthquakes in the Cocos plate (Oaxaca, 1999, **M** 7.5), the Philippine Sea plate (Geiyo, 2001, **M** 6.7) and the Juan de Fuca plate (Nisqually, 2001, **M** 6.8) are inferred to have occurred close to the slab Moho [e.g., *Wang et al.*, 2004a]. All nine earthquakes from Table 2 having a $\mathbf{M} > 4$ have a velocity of 7.8–8.1 km/s at the hypocenter and are located between 40 and 55 km depth (Table 3). The seismic velocity at these hypocenters indicate that they most likely originate in the nearly fully eclogitized crust and/or close to the subducting slab Moho. This observation is consistent with the slab depth contours (Figure 11) of *McCrory et al.* [2004].

Our findings that large inslab earthquakes in the Juan de Fuca plate occur close to the slab Moho are consistent with the hypothesis of *Wang et al.* [2004a]. *Wang et al.* [2004a] proposed that there is a tendency for large inslab earthquakes to occur deep inside the slab. They argued that crustal densification in the upper few hundred meters of the slab crust will shatter the crust resulting in only smaller magnitude earthquakes. They proposed that dehydration along the existing faults in the slab's lower crust and upper mantle can facilitate seismic rupture that can propagate for large distances, resulting in large earthquakes.

6. Summary

Our regional 3-D P-wave velocity model presents the first regional high-resolution image of the northern Cascadia subduction zone beneath S.W. British Columbia and N.W.

Washington state. The mega-thrust zone above the Juan de Fuca plate is characterized by broad zone of low velocities of 6.4–6.6 km/s at 25–35 km depth in the region that lies down dip of the mega-thrust locked zone. This low velocity zone is virtually aseismic but lies within the region experiencing episodic tremor and slip. This region also coincides with high electrical conductivity region mapped in previous magneto-telluric studies, a landward dipping band of seismic reflectors, and a low shear velocity layer modeled in receiver function studies. These low velocities are inferred to be due to either trapped fluids, highly sheared lower crustal rocks, and/or underthrust accretionary rocks.

A broad low velocity zone in the forearc mantle having velocities between 7.2 and 7.5 km/s, imaged at depths of 37–45 km above the Juan de Fuca plate, is inferred to reflect a serpentinized upper mantle. This zone is similar in velocity to the low velocity zones observed in the forearc mantle beneath central Japan, northern Costa Rica, eastern Aleutians, and the Andes. The younger sedimentary basins in the Strait of Georgia and Puget Sound are imaged above the zone of inferred forearc mantle serpentinization.

The largest inslab earthquakes, having a $\mathbf{M} > 4$ and occurring at depths between 40 and 55 km, are inferred to originate close to the Moho of the subducting slab. Earthquakes occurring closer to the slab Moho are probably not limited in size by the thickness of the slab crust and the faulting could extend from the slab crust into the slab upper mantle with larger rupture surfaces than earthquakes restricted solely to the crust of the subducting slab.

Acknowledgments. We are thankful to Tom Van Wagoner for sharing the earthquake travel time picks from his study. This research was supported by Earthquake Program

of the U.S. Geological Survey. All figures were made using the *Generic Mapping Tools* [*Wessel and Smith*, 1991, 1995].

References

Atwater, B.F., and E. Hemphill-Haley (1997), Recurrence intervalsfor great earthquakesof the past 3500 years at northeastern Willapa Bay, Washington. *U.S. Geological Survey Professional Paper 1576*.

Brandon, M. T. and A. R. Calderwood (1990), High–pressure metamorphism and uplift of the Olympic subduction complex, *Geology*, *18*, 1252–1255.

Brocher, T. M. and N. I. Christensen (2001), Density and velocity relationships for digital sonic and density logs from coastal Washington and laboratory measurements of Olympic peninsula mafic rocks and greywackes, *Open-File Report 01–264*, U.S. Geological Survey, http://geopubs.wr.usgs.gov/open-file/of01-264/.

Brocher, T. M., T. Parsons, R. A. Blakely, N. I. Christensen, M. A. Fisher, R. E. Wells, and the SHIPS Working Group (2001), Upper crustal structure in Puget Sound, Washington: Results from 1998 Seismic Hazards Investigation of Puget Sound, *J. Geophy. Res.*, *106*, 13541–13564.

Brocher, T. M., T. Parsons, K. C. Creager, R. S. Crosson, N. P. Symons, G. D. Spence, B. C. Zelt, P. T. C. Hammer, R. D. Hyndman, D. C. Mosher, A. M. Tréhu, K. C. Miller, R. S. ten Brink, M. A. Fisher, T. L. Pratt, M. G. Alvarez, B. C. Beaudoin, K. E. Louden, and C. S. Weaver (1999), Wide–angle seismic recordings from the 1998 Seismic Hazards Investigation Of Puget Sound (SHIPS), Western Washington and British Colombia, *Open-File Report 99–314*, U.S. Geological Survey, http://geopubs.wr.usgs.gov/open-

file/of99-314/.

Calvert, A. J. (2004), Seismic reflection imaging of two megathrust shear zones in the northern Cascadia subduction zone, *Nature*, *428*, 163–167.

Calvert, A. J. and R. M. Clowes (1990), Deep, high-amplitude reflections from a major shear zone above the subducting Juan de Fuca plate. *Geology*, *18*, 1091–1094.

Cassidy, J. F. (1995), A comparison of the receiver structure beneath stations of the Canadian National Seismograph Network, *Can. J. Earth Sci.*, *32*, 938–951.

Cassidy, J. F. and R. M. Ellis (1991), Shear wave constraints on a deep crustal reflective zone beneath Vancouver Island. *J. Geophys. Res. 96*, 19843–19851.

Cassidy, J. F. and R. M. Ellis (1993), S-wave velocity structure of the northern Cascadia subduction zone, *J. Geophys. Res. 98*, 4407–4421.

Cassidy J. F., and F. Waldhauser (2003), Evidence for both crustal and mantle earthquakes in the subducting Juan de Fuca plate, *Geophys. Res. Lett.*, *30*, 1095, doi:10.1029/2002GL015511.

Clague, J. J., (1997), Evidence for large earthquakes at the Cascadia subduction zone, *Reviews of Geophysics*, *35*, 439–460.

Clowes, R. M., M. T. Brandon, A. G. Green, C. J. Yorath, A. Sutherland-Brown, E. R. Kanasewich, and C. S. Spencer (1987), LITHOPROBE southern Vancouver Island: Cenozoic subduction complex imaged by deep seismic reflections, *Can. J. Earth Sci.*, *24*, 31–51.

Currie C. A., R. D. Hyndman, K. Wang, and V. Kostoglodov (2002), Thermal models of the Mexico subduction zone: Implications for the megathrust seismogenic zone, *J. Geophys. Res.*, *107*, 2370, doi:10.1029/2001JB000886.

Dragert, H., K. Wang and T. S. James (2001), A Silent Slip Event on the Deeper Cascadia Subduction Interface, *Science 292*, 1525–1528.

Drew, J.J., and R.M. Clowes (1990), A re-interpretation of the seismic structure across the active subduction zone of western Canada, in *Studies of laterally heterogeneous structures using seismic refraction and reflection data, Proceedings of the 1987 Commission on Controlled Source Seismology Workshop*, *Edited by* Green, A.G., Geological Survey of Canada, Paper 89-13: 115–132.

Fisher, M. A., et al. (1999), Seismic survey probes urban earthquake hazards in Pacific Northwest, *Eos, Trans. AGU*, *80(2)*, 13–17.

Hacker B. R., S. M. Peacock, G. A. Abers, and S. D. Holloway (2003), Subduction factory 2. Are intermediate-depth earthquakes in subducting slabs linked to metamorphic dehydration reactions?, *J. Geophys. Res.*, *108* , 2030, doi:10.1029/2001JB001129.

Hyndman, R. D. (1988), Dipping seismic reflectors, electrically conductive zones, and trapped water in the crust over a subducting plate, *J. Geophys. Res.*, *93*, 13391–13405.

Hyndman, R. D., and K. Wang (1995), The rupture zone of Cascadia great earthquakes from current deformation and the thermal regime, *J. Geo phys. Res.*, *100*, 22133–22154, doi:10.1029/95JB01970.

Hyndman, R. D., C. J. Yorath, R. M. Clowes, and E. E. Davis (1990), The northern Cascadia Subduction Zone at Vancouver Island: Seismic structure and tectonic history, *Can. J. Earth Sci.*, *27*, 313–329.

Hyndman R. D., S. Mazzotti, D. Weichert, and G. C. Rogers (2003), Frequency of large crustal earthquakes in Puget Sound and Southern Georgia Strait predicted from geodetic and geological deformation rates, *J. Geophys. Res.*, *108*, 2033,

doi:10.1029/2001JB001710.

Johnson, S. Y., (1984), Evidence for a margin truncating transcurrent fault (pre–late Eocene) in western Washington, *Geology*, *12*, 538–541.

Johnson, S. Y., (1985), Eocene strike-slip faulting and nonmarine basin formation in Washington, in Strike-Slip Deformation, Basin Formation, and Sedimentation, no. 37, edited by K. T. Biddle and N. Christie-Blick, *Spec. Pub. Soc. Econ. Paleon. Mineral.*, 283–302.

Johnson, S. Y., C. J. Potter, and J. M. Armentrout (1994), Origin and evolution of the Seattle Fault and Seattle Basin, Washington, *Geology*, it 22, 71–74.

Jones, D. L., N. J. Silberling, and J. Hillhouse (1977), Wrangellia - a displaced terrane in northwestern North America, *Can. J. Earth Sci.*, *14*, 2565–2577.

Kao, H., S.-Ju. Shan, G. Rogers, H. Dragert, J. F. Cassidy, and K. Ramachandran (2005), Depth distribution of seismic tremors along the northern Cascadia margin, *Nature*, *436*, 841–844, doi:10.1038/nature03903

Kirby, S.H., E.R., Engdahl, and R., Denlinger (1996), Intraslab earthquakes and arc volcanism: Dual physical expressions of crustal and uppermost mantle metamorphism in subducting slabs, in *Subduction: Top to bottom*, *Edited by* G.E. Bebout, D.W. Scholl, S.H. Kirby, and J.P. Platt, American Geophysical Union, Geophysical Monograph, *96*, 195-214.

McCrory, P.A., J. L. Blair, D.H. Oppenheimer, and S. R. Walter (2004), Depth to the Juan de Fuca slab beneath the Cascadia subduction margin – A 3–D model for sorting earthquakes, U.S. Geological Survey Data Series 91, http://pubs.usgs.gov/ds/91.

Miller, K. C., G. R. Keller, J. M. Gridley, J. H. Luetgert, W. D. Mooney, and H. Thybo (1997), Crustal structure along the west flank of the Cascades, western Washington, *J. Geophys. Res.*, *102*, 17857–17873.

Monger, J. W. H. (1990), Georgia Basin - regional setting and adjacent Coast Mountains geology, British Columbia, *Current Research, Part F, Paper 90-1F*, 95–108, Geological Survey Canada.

Monger, J. W. H., R. A. Price, and D. J. Tempelman–Kluit (1982), Tectonic accretion and the origin of the two major metamorphic and plutonic welts in the Canadian Cordillera, *Geology*, *10*, 70–75.

Muller, J. E. (1977), Evolution of the Pacific Margin, Vancouver Island, and adjacent regions, *Can. J. Earth Sci.*, *14*, 2062–2085.

Nicholson, T. A., Bostock, M. G., and Cassidy, J. F. (2005), New constraints on subduction zone structure in northern Cascadia, *Geophy. J. Int.*, *161*, doi:10.1111/j.1365-246X.2005.02605.x.

Nedimović, M. R., R. D. Hyndman, K. Ramachandran, and G. D. Spence (2003), Reflection signature of seismic and aseismic slip on the northern Cascadia subduction interface, *Nature*, *424*, 416–420.

Peacock, S.M. (1993), Large-scale hydration of the lithosphere above subducting slabs, *Chemical Geology*, *108*, 49–59.

Peacock, S.M. (2001), Are double seismic zones caused by serpentine dehydration reactions in subducting oceanic mantle? *Geology*, *29*, 299–302.

Peacock, S.M., and K. Wang (1999), Seismic consequences of warm versus cool subduction zone metamorphism: Examples from northeast and southwest Japan, *Science*, *286*, 937–

939.

Peacock, S. M., K. Wang, and A. M. McMahon (2002), Thermal structure and metamorphism of subducting oceanic crust: Insight into Cascadia inslab earthquakes, *In* The Cascadia Subduction Zone And Related Subduction Systems - Seismic Structure, Intraslab Earthquakes and Processes, and Earthquake Hazards, *Edited by* Stephen Kirby, Kelin Wang and Susan Dunlop, *Open-File Report 02328*, 123–126, U.S. Geological Survey, http://geopubs.wr.usgs.gov/open-file/of02-328/.

Pratt, T. L., T. M. Brocher, C. S. Weaver, K. C. Miller, A. M. Trehu, K. C. Creager, R. S. Crosson, and , C. M. Snelson (2003), Amplication of seismic waves by the Seattle basin, northwestern U. S., *Bulletin of the Seismological Society of America*, *93*, 533–545

Preston, L. A., K. C. Creager, R. S. Crosson, T. M. Brocher, and A. M Tréhu (2003), Intraslab Earthquakes: Dehydration of the Cascadia Slab, *Science*, *302*, 1197–1200.

Ramachandran, K., (2001), Velocity structure of S.W. British Columbia and N.W. Washington from 3-D non-linear seismic tomography, Ph.D. thesis, University of Victoria, Victoria, BC, Canada.

Ramachandran K., S. E. Dosso, C. A. Zelt, G. D. Spence, R. D. Hyndman, T. M. Brocher (2004), Upper crustal structure of southwestern British Columbia from the 1998 Seismic Hazards Investigation in Puget Sound, *J. Geophys. Res.*, *109*, B09303, doi:10.1029/2003JB002826.

Ramachandran, K., S. E. Dosso, G. D. Spence, R. D. Hyndman, and T. M. Brocher (2005), Forearc structure beneath southwestern British Columbia: A three-dimensional tomographic velocity model, *J. Geophys. Res.*, *110*, B02303, doi:10.1029/2004JB003258.

Riddihough, R. P., and R. D. Hyndman (1991), Modern plate tectonic regime of the continental margin of western Canada, in *Geology of North America, vol. G-2, Geology of the Cordilleran Orogen in Canada*, edited by H. Gabrielse and C. J. Yorath, Geology of Canada, 4, 435-455, Geol. Surv. of Can., Ottawa, Ontario, Canada.

Rogers, G. C. (1983), Seismotectonics of British Columbia, Ph.D. Thesis, University of British Columbia, Vancouver, Canada.

Rogers, G. C., (1998), Earthquakes and earthquake hazard in the Vancouver area; in Geology and Natural Hazards of the Fraser River Delta, British Columbia, *Edited by* J.J. Clague, J.L. Luternauer, and D.C. Mosher, *Geol. Surv. Can. Bull.*, *525*, 17–25.

Rogers, G. C., (2002), The role of phase changes in the development of forearc basins, *In* The Cascadia Subduction Zone And Related Subduction Systems - Seismic Structure, Intraslab Earthquakes and Processes, and Earthquake Hazards, *Edited by* Stephen Kirby, Kelin Wang and Susan Dunlop, *Open-File Report 02328*, 147, U.S. Geological Survey, http://geopubs.wr.usgs.gov/open-file/of02-328/.

Rogers, G.C. and H. Dragert (2003), Episodic tremor and slip on the Cascadia subduction zone: the chatter of silent slip, *Science*, *300*, 1942–1943.

Satake, K., K. Shimazaki, Y. Tsuji, and K. Ueda (1996), Time and size of a great earthquake in Cascadia inferred from Japanese tsunami records of January 1700, *Nature*, *379*, 246-249.

Smith, P. L., and H. W. Tipper (1986), Plate tectonics and palobiogeography: Early Jurassic (Pliensbachian) endemism and diversity, *Palaios*, it 1, 399–412.

Snavely, P. D., Jr., (1987), Tertiary geologic framework, neotectonics, and petroleum potential of the Oregon-Washington continental margin, *in* Scholl, D.W., Grantz, A., and

Vedder, J. G., eds., Geology and resource potential of the continental margin of western North America and adjacent ocean basinsBeaufort Sea to Baja California: Houston, Texas, *Circum-Pacific Council for Energy and Mineral Resources, Earth Science Series*, *6*, 305–335.

Tabor, R. W. (1994), Late Mesozoic and possible early Tertiary accretion in western Washington statethe Helena-Haystack melange and the Darrington-Devils Mountain fault zone, *Geol. Soc. Am. Bull.*, *106*, 217–232.

Tabor, R. W., and W. M. Cady (1978), The structure of the Olympic Mountains, Washington-analysis of a subduction zone, *U.S. Geol. Surv. Prof. Pap.*, *1033*.

Tréhu, A. M., T. M. Brocher, K. C. Creager, M. A. Fisher, L. Preston, and G. D. Spence (2002), Geometry of the subducting Juan de Fuca Plate: New constraints from SHIPS98, *In* The Cascadia Subduction Zone And Related Subduction Systems - Seismic Structure,Intraslab Earthquakes and Processes, and Earthquake Hazards, *Edited by* Stephen Kirby, Kelin Wang and Susan Dunlop, *Open-File Report 02328*, 25–32, U.S. Geological Survey, http://geopubs.wr.usgs.gov/open-file/of02-328/.

Van Wagoner, T. M., R. S. Crosson, K. C. Creager, G. F. Medema, L. A. Preston, N. P. Symons, and T. M. Brocher (2002), Crustal structure and relocated earthquakes in the Puget Lowland, Washington from high resolution seismic tomography, *J. Geophys. Res.*, *107*(B12), 10.10129/2001JB000710.

Wada, I., K. Wang, and Y. Ishikawa (2004), Stress and Metamorphic Conditions for Warm-slab Earthquakes: Geiyo Area, Southwest Japan, *Eos Trans. AGU*, *85(17)*, Jt. Assem. Suppl., Abstract S32A-06.

Wang, K., T. Mulder, G. C. Rogers, and R. D. Hyndman (1995), Case for low coupling stress on the Cascadia subduction fault, *J. Geophys. Res.*, *100*, 12907–12918.

Wang K., J. F. Cassidy, I. Wada, A. J. Smith (2004a), Effects of metamorphic crustal densification on earthquake size in warm slabs, *Geophys. Res. Lett.*, *31*, L01605, doi:10.1029/2003GL018644.

Wang K., I. Wada, Y. Ishikawa (2004b), Stresses in the subducting slab beneath southwest Japan and relation with plate geometry, tectonic forces, slab dehydration, and damaging earthquakes, *J. Geophys. Res.*, *109*, B08304, doi:10.1029/2003JB002888.

Zelt, B. C., R. M. Ellis, C. A. Zelt, R. D. Hyndman, C. Lowe, G. D. Spence, and M. A. Fisher (2001), Three dimensional crustal velocity structure beneath the Strait of Georgia, British Columbia, *Geophys. J. Int.*, *144*, 695–712.

Zelt, C. A. and P. J. Barton (1998), 3–D Seismic refraction tomography: A comparison of two methods applied to data from the Faroe basin, *J. Geophys. Res.*, *103*, 7187–7210.

Table 1. Distribution of the deep earthquakes (> 35 km depth) in different depth intervals classified by the P-wave velocity values at the hypocenter

Depth Range (km)	Number of earthquakes in the P-wave velocity range 6.8–7.2	7.2–7.8	7.8–8.2
35–40	9	27	26
40–50	5	32	91
50–60	0	24	72
60–70	0	0	30
70–80	0	0	7
80–95	0	0	1

Table 2. Distribution of deep earthquakes (> 35 km depth) in different magnitude intervals classified by the P-wave velocity values at the hypocenter.

	Number of earthquakes in the P-wave velocity range		
Magnitude	6.8–7.2	7.2–7.8	7.8–8.2
$1 < M < 2$	10	49	88
$2 < M < 3$	4	31	104
$3 < M < 4$	0	3	27
$4 < M < 5$	0	0	6
$5 < M < 6$	0	0	2
≥ 6	0	0	1

Notes: Earthquakes of $\mathbf{M} > 4$ are inferred to occur close to the slab Moho

Table 3. Depth, magnitude and P-wave velocity at the hypocenter for the earthquakes of $\mathbf{M} > 4$) from Table 2.

No.	Lat./Lon.	Depth (km)	Mag.	Velocity at the hypocenter (km/s)
1	47.9649/-123.0160	48.8	4.2	8.0
2	47.3325/-123.2320	43.8	4.3	8.1
3	47.8148/-123.3430	46.0	4.5	7.8
4	47.4051/-122.7820	46.2	4.4	7.8
5	47.4117/-123.1610	45.4	4.0	8.1
6	47.0815/-122.6880	52.9	4.3	8.0
7	47.0670/-123.4460	41.1	5.8	7.8
8	47.1638/-123.4950	41.1	5.0	7.8
9	47.1440/-122.7220	52.4	6.8	7.9

Notes: The above earthquakes are inferred to occur close to the slab Moho. See Figure 11 for the location map of the above earthquakes

FIGURE CAPTIONS

Figure 1. Location map showing the SHIPS temporary land based receiving stations (blue triangles) and air-gun shot positions (red lines) of the active source data used in the present study. Bottom left inset shows the earthquakes (blue stars) and permanent recording stations (red triangles) used in this study. Inset to the right top shows the plate tectonic regime of the study area.

Figure 2. Sedimentary basin and fault map. CFTB-Cowichan Fold and Thrust Belt; CH-Chuckanut sub-basin; CLB-Clallam basin; CPC-Coast Plutonic Complex; CRBF-Coast Range boundary fault; CR-Crescent terrane; DDMF-Darrington-Devils Mountain fault; EB-Everett basin; HCF-Hood Canal fault; HRF-Hurricane Ridge fault; KA-Kingston Arch; LIF-Lummi Island fault; LRF-Leech River fault; B-Muckleshoot Basin; NA- Nanaimo sub-basin; OF-Olympia fault; OIF-Outer Islands fault; PB-Possesion Basin; PR-Pacific Rim terrane; PTB-Port Townsend basin; SB-Seattle basin; SF-Seattle fault; SJF-San Juan fault; SMF-Survey Mountain fault; SQB-Sequim basin; SQF-Sequim fault; SU-Seattle uplift; SWIF-southern Whidbey Island fault; TB-Tacoma basin; TF-Tacoma fault; WA-Whatcom sub-basin. AB, CD, EF, GH, IJ, KL, MN, NO, PQ, and QR show the location of the vertical cross-sections shown in Figures 6, 7, and 8. ALB and LAS are receiver function study locations from *Cassidy and Ellis* [1993].

Figure 3. (a) Travel-time misfit of active source data for initial 1-D velocity model, (b) travel-time misfit of active source data for final velocity model , c) Travel-time misfit of earthquake data for initial 1-D velocity model and (d) travel-time misfit of earthquake data for final velocity model.

Figure 4. Depth slices at 3, 9, 15, 21 and 27 km depth of (a) ray hit count, (b) checkerboard test recovered anomaly pattern and (c) semblance values, for 30 km grid size.

Figure 5. Depth slices at 21, 39, 45, 51 and 57 km depth of (a) ray hit count, (b) checkerboard test recovered anomaly pattern, and (c) semblance values, for 50 km grid size.

Figure 6. Vertical cross-section a) AB, b) CD, and c) EF. The cross-sections are approximately in the margin perpendicular direction. Location of the cross-sections on Figure 2. Abbreviations are as in Figure 2.

Figure 7. Vertical cross-section a) GH, b) IJ, and c) KL. The cross-sections are approximately in the margin perpendicular direction. Location of the cross-sections on Figure 2. Abbreviations are as in Figure 2.

Figure 8. Vertical cross-section a) PQ and QR and b) MN and NO. The cross-sections are approximately in the margin parallel direction. Location of the cross-sections on Figure 2. Abbreviations are as in Figure 2.

Figure 9. Horizontal cross-sections at a) 27 km, b) 33 km, c) 36 km, d) 45 km, e) 51 km, and f) 57 km depth.

Figure 10. a) Horizontal cross-section at 3 km depth showing the outline of sedimentary basins. b) Gravity anomaly map (data from the National Geophysical Data Center, USA CD-ROM). The thick red dashed line marks the approximate position of the junction of the subducting Juan de Fuca crust and the forearc mantle wedge. Abbreviations are as in Figure 2.

Figure 11. Location of the nine earthquakes (**M** > 4) inferred to originate close to the slab Moho (Table 3) are shown by the stars. The depth to the top of the oceanic Moho is shown by the dashed line contours computed from the slab depth values (km) from *McCrory et al.* [2004] by adding an average oceanic crustal thickness of 7 km. Beneath southern Vancouver Island, the slab depth and hence oceanic Moho depth contours are modified according to the results inferred from the present study.

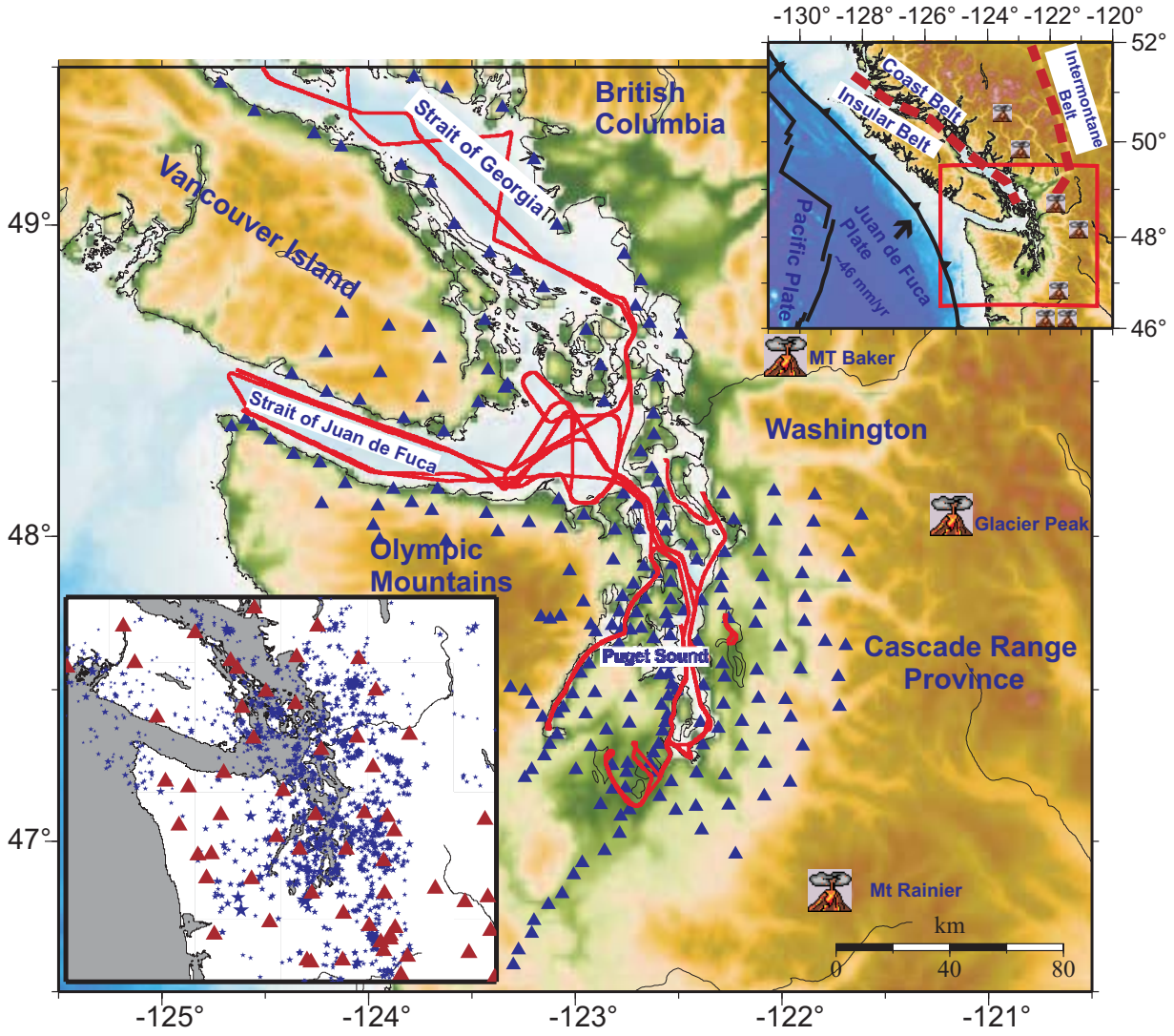
British Columbia
Strait of Georgia
Vancouver Island
Strait of Juan de Fuca
Olympic Mountains
Puget Sound
Washington
Glacier Peak
Cascade Range Province
Mt Rainier
MT Baker
km
0
40
80
49°
48°
47°
-125°
-124°
-123°
-122°
-121°
-130° -128° -126° -124° -122° -120°
52°
50°
48°
46°
Coast Belt
Insular Belt
Intermontane Belt
Pacific Plate
Juan de Fuca Plate
46 mm/yr

Figure 1

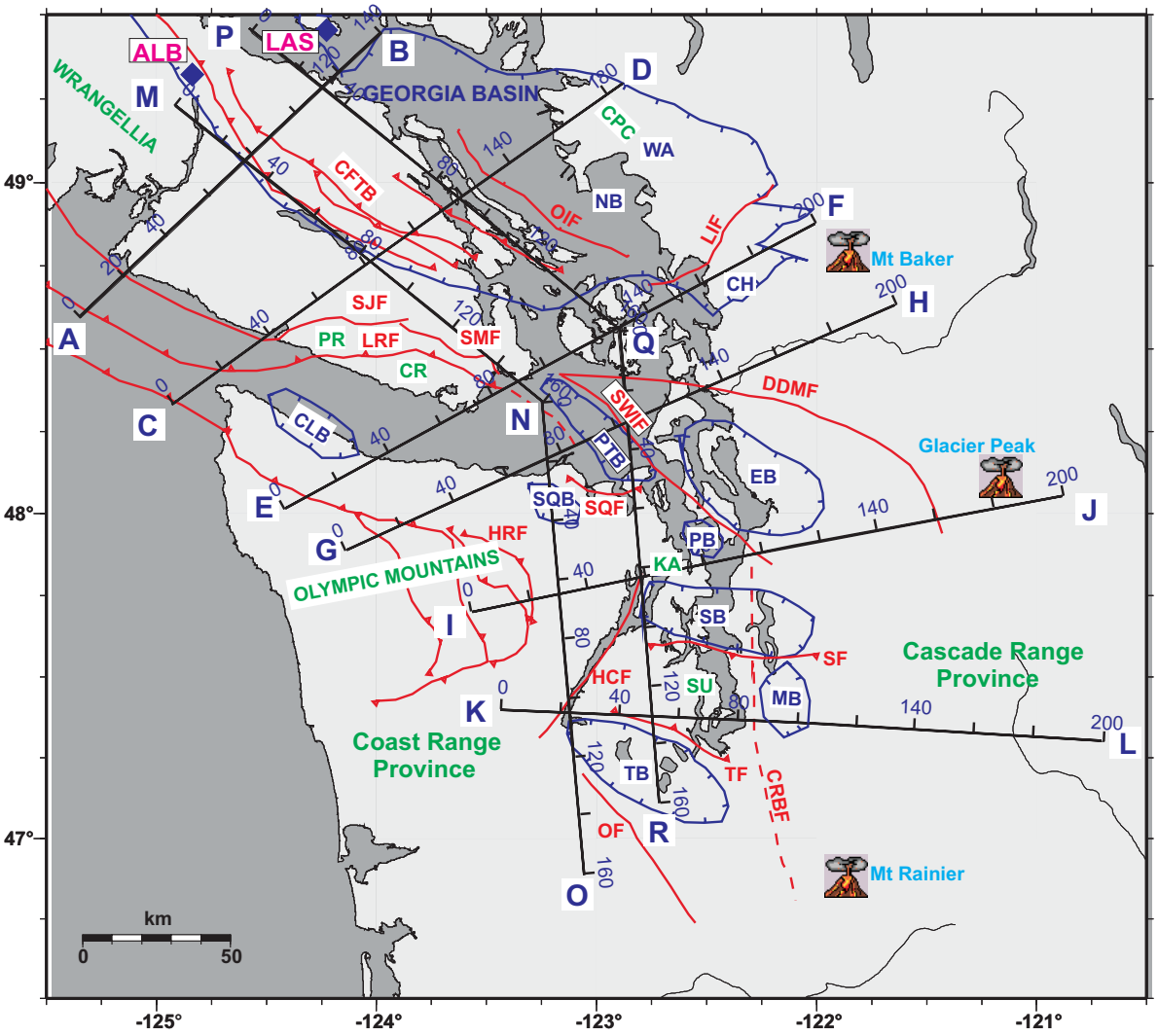
ALB
LAS
P
B
D
M
WRANGELLIA
GEORGIA BASIN
CPC
WA
CFTB
NB
OIF
LIF
F
Mt Baker
CH
H
SJF
A
PR
LRF
SMF
Q
CR
DDMF
C
CLB
N
SWIF
PTB
Glacier Peak
EB
E
SQB
SQF
J
G
HRF
PB
OLYMPIC MOUNTAINS
KA
I
SB
SF
Cascade Range Province
HCF
SU
MB
K
Coast Range Province
TB
TF
CRBF
L
OF
R
O
Mt Rainier
km
0
50
49°
48°
47°
-125°
-124°
-123°
-122°
-121°

Figure 2

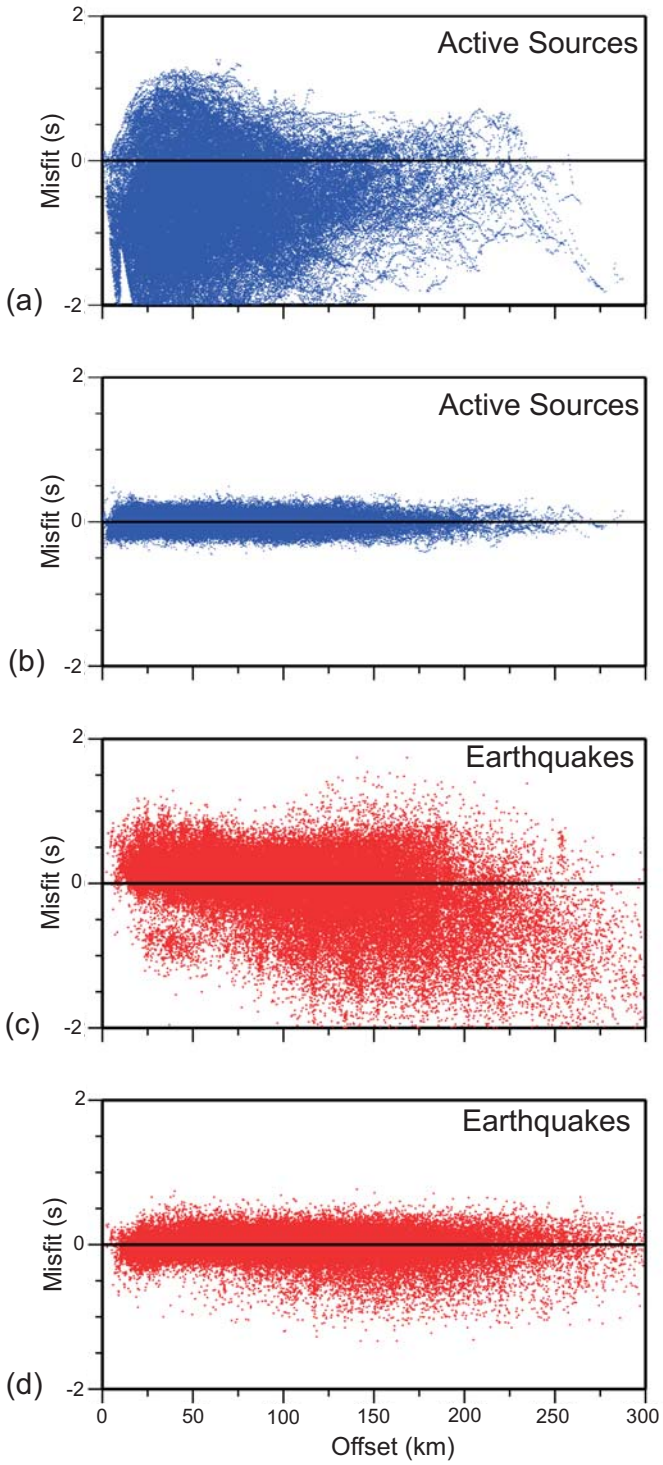
Active Sources
Misfit (s)
(a)
Active Sources
Misfit (s)
(b)
Earthquakes
Misfit (s)
(c)
Earthquakes
Misfit (s)
(d)
2
0
-2
0
50
100
150
200
250
300
Offset (km)

Figure 3

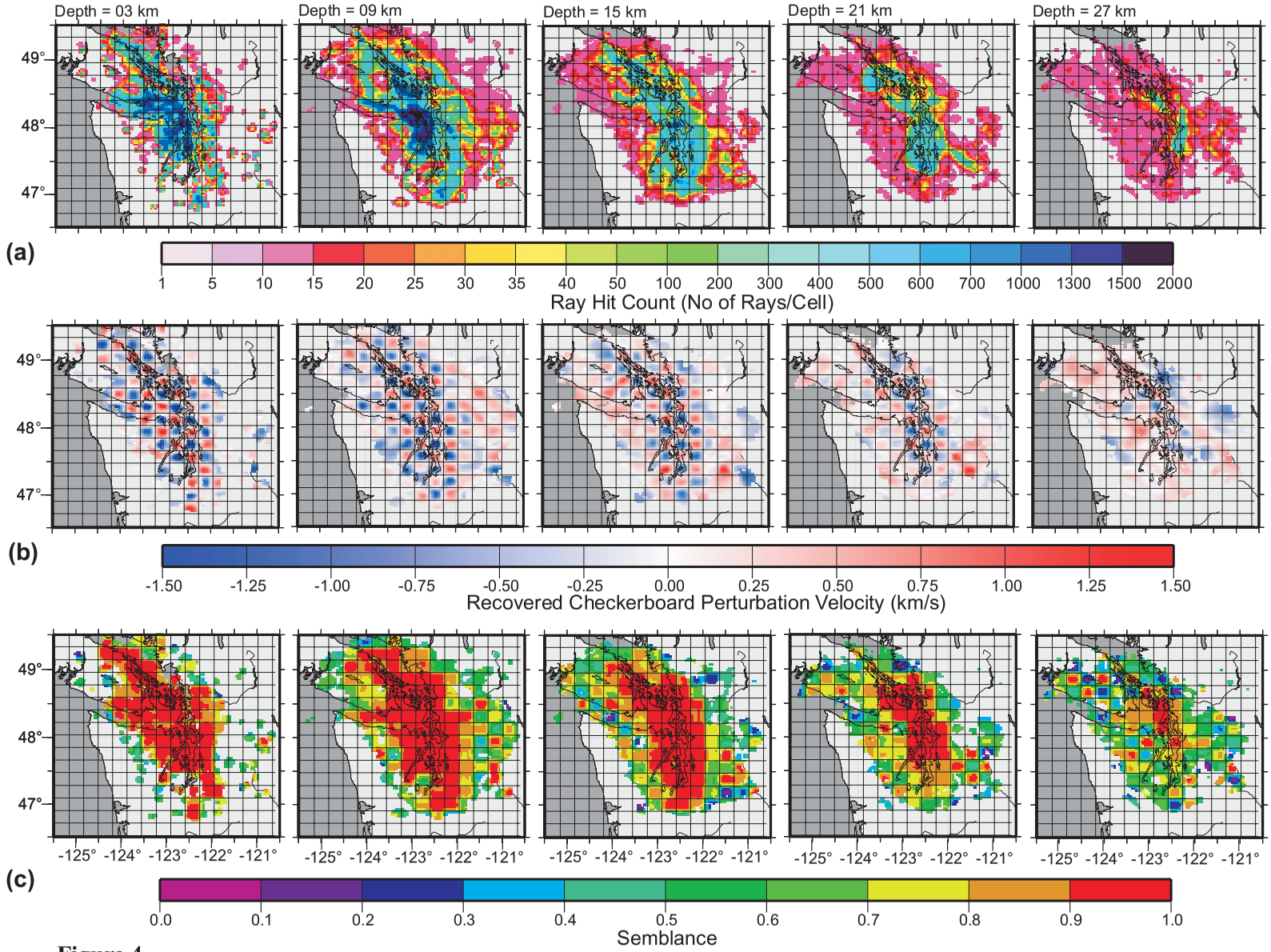
Depth = 03 km
Depth = 09 km
Depth = 15 km
Depth = 21 km
Depth = 27 km
49°
48°
47°
(a)
1 5 10 15 20 25 30 35 40 50 100 200 300 400 500 600 700 1000 1300 1500 2000
Ray Hit Count (No of Rays/Cell)
(b)
-1.50 -1.25 -1.00 -0.75 -0.50 -0.25 0.00 0.25 0.50 0.75 1.00 1.25 1.50
Recovered Checkerboard Perturbation Velocity (km/s)
(c)
-125° -124° -123° -122° -121°
0.0 0.1 0.2 0.3 0.4 0.5 0.6 0.7 0.8 0.9 1.0
Semblance

Figure 4

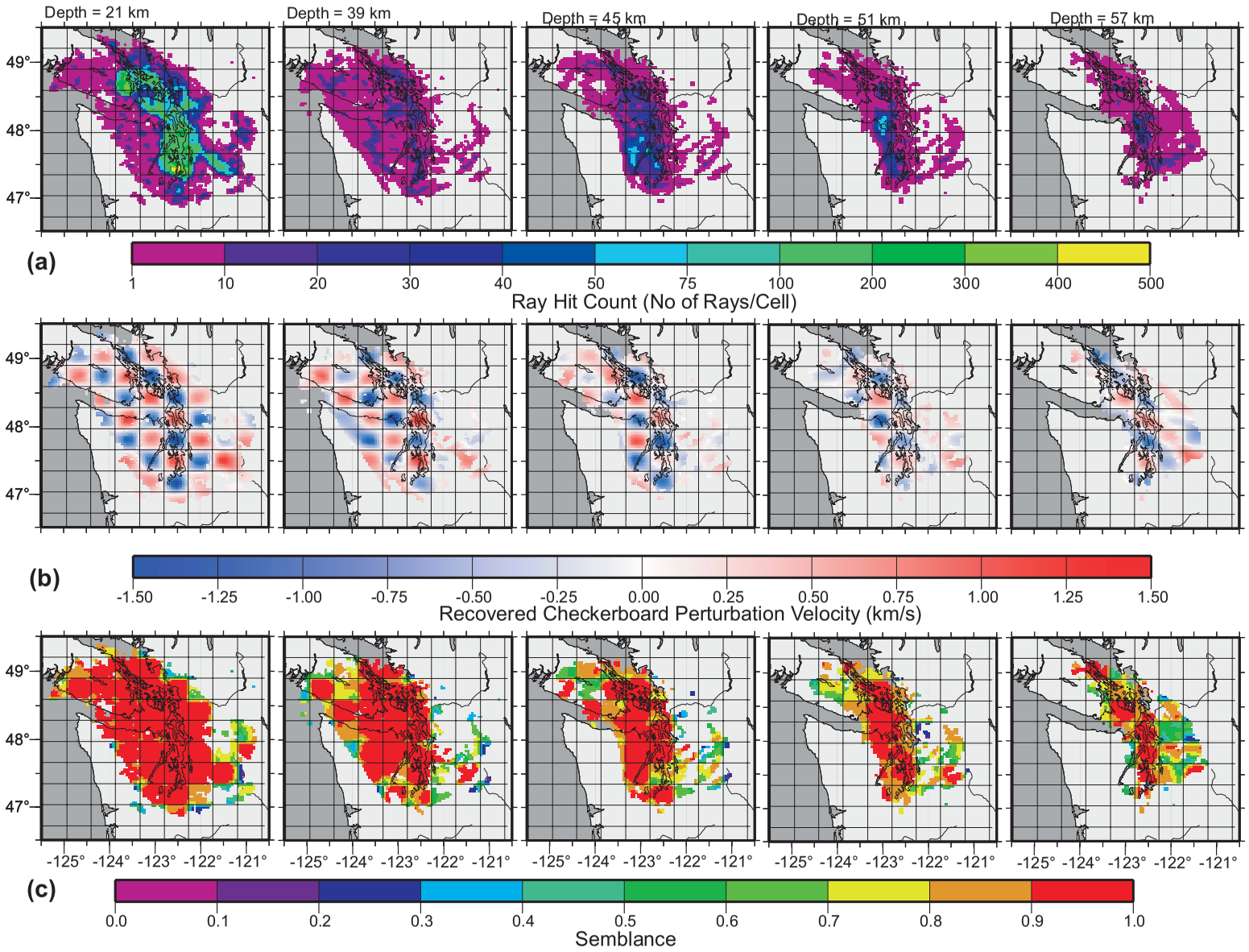
Depth = 21 km
Depth = 39 km
Depth = 45 km
Depth = 51 km
Depth = 57 km
49°
48°
47°
(a)
1
10
20
30
40
50
75
100
200
300
400
500
Ray Hit Count (No of Rays/Cell)
(b)
-1.50
-1.25
-1.00
-0.75
-0.50
-0.25
0.00
0.25
0.50
0.75
1.00
1.25
1.50
Recovered Checkerboard Perturbation Velocity (km/s)
-125° -124° -123° -122° -121°
(c)
0.0
0.1
0.2
0.3
0.4
0.5
0.6
0.7
0.8
0.9
1.0
Semblance

Figure 5

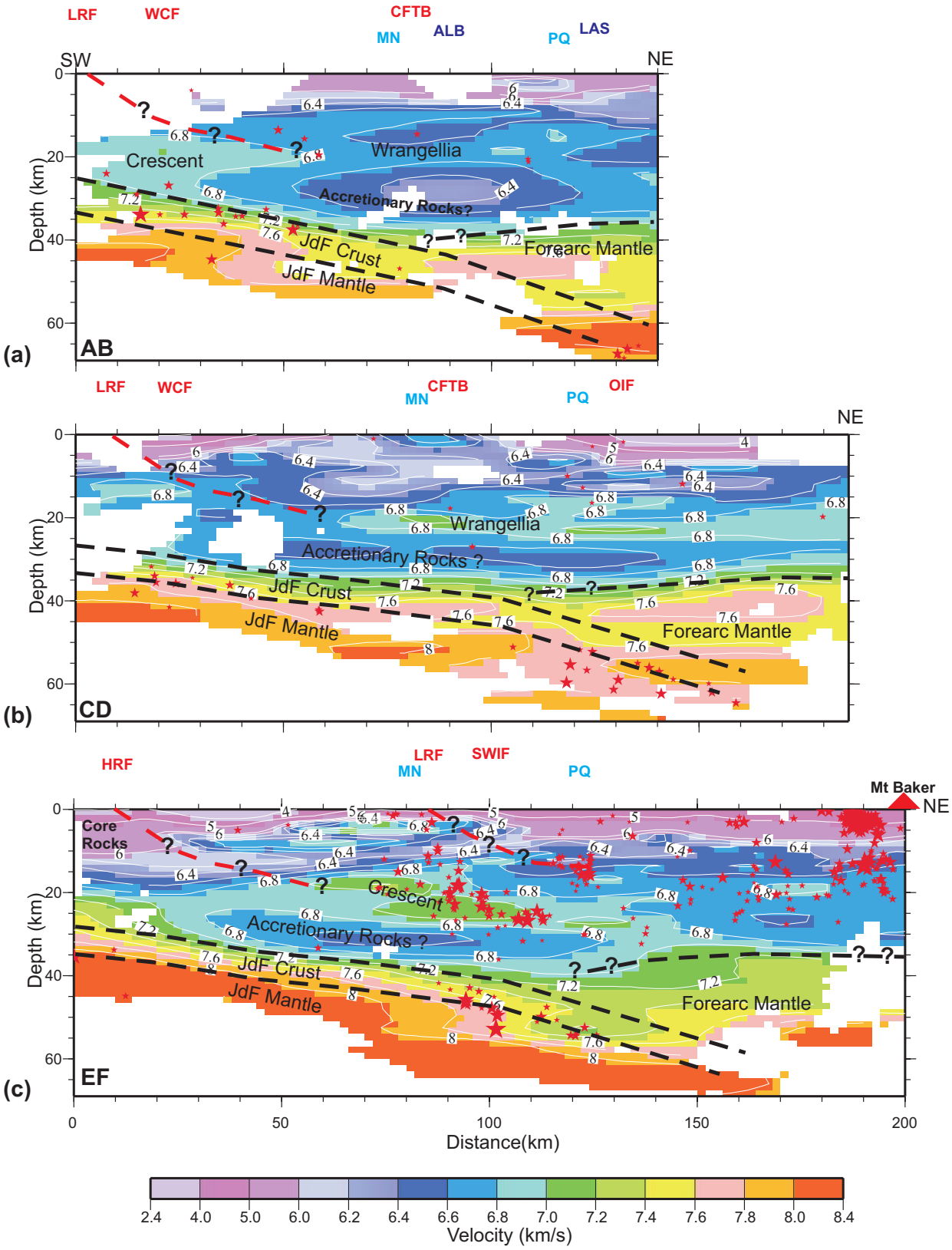
LRF
WCF
CFTB
MN
ALB
PQ
LAS
SW
NE
Crescent
Wrangellia
Accretionary Rocks?
JdF Crust
JdF Mantle
Forearc Mantle
Depth (km)
(a)
AB
LRF
WCF
CFTB
MN
PQ
OIF
NE
Wrangellia
Accretionary Rocks ?
JdF Crust
JdF Mantle
Forearc Mantle
(b)
CD
HRF
LRF
SWIF
MN
PQ
Mt Baker
NE
Core Rocks
Crescent
Accretionary Rocks ?
JdF Crust
JdF Mantle
Forearc Mantle
(c)
EF
Distance(km)
Velocity (km/s)

Figure 6

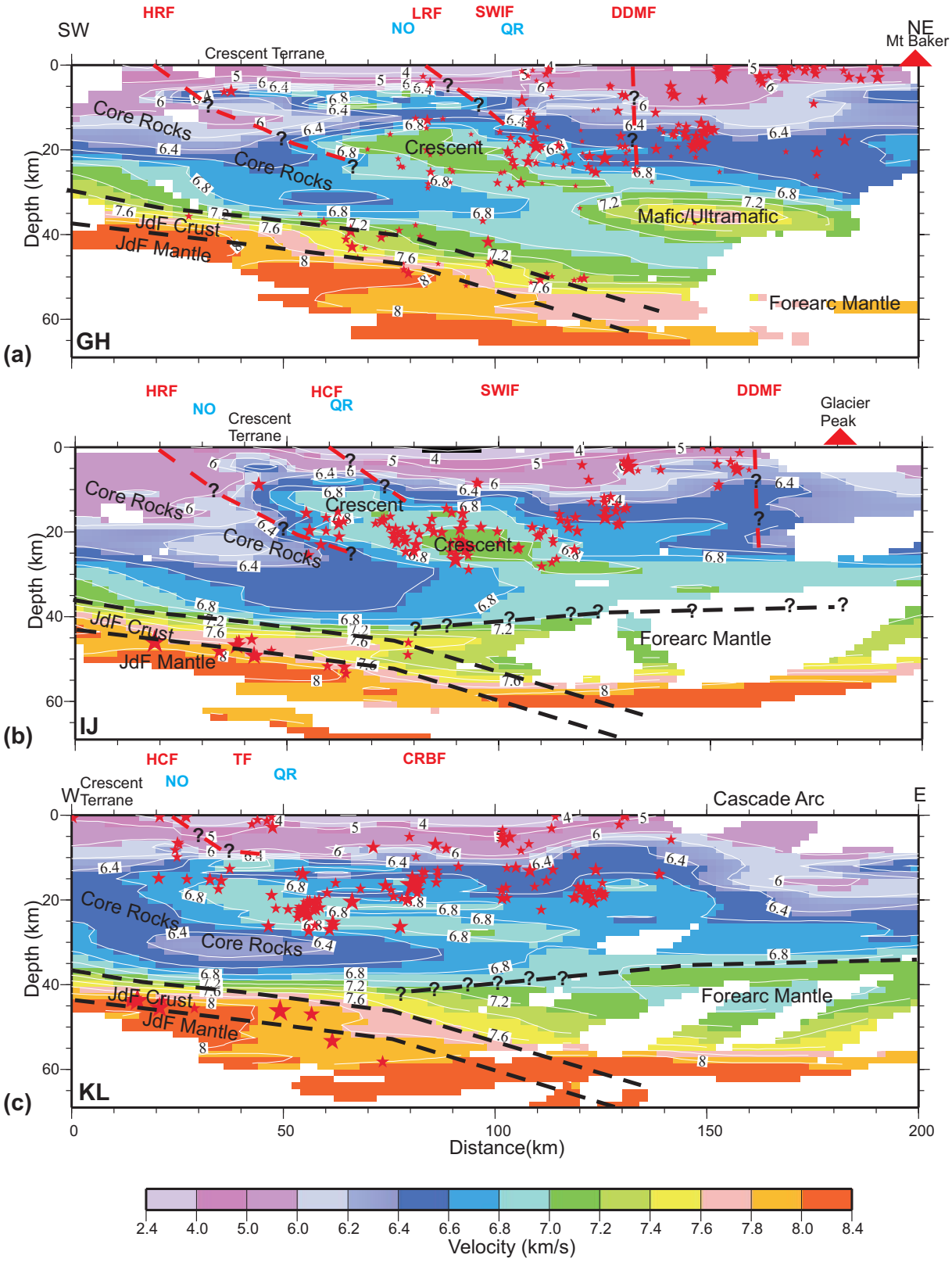
SW
NE
HRF
LRF
SWIF
DDMF
NO
QR
Mt Baker
Crescent Terrane
Core Rocks
Crescent
Core Rocks
Mafic/Ultramafic
JdF Crust
JdF Mantle
Forearc Mantle
GH
(a)
Depth (km)
HRF
NO
HCF
QR
SWIF
DDMF
Glacier Peak
Crescent Terrane
Core Rocks
Crescent
Core Rocks
Crescent
JdF Crust
JdF Mantle
Forearc Mantle
IJ
(b)
HCF
TF
QR
CRBF
W
Crescent Terrane
NO
Cascade Arc
E
Core Rocks
Core Rocks
JdF Crust
JdF Mantle
Forearc Mantle
KL
(c)
Distance(km)
Velocity (km/s)

Figure 7

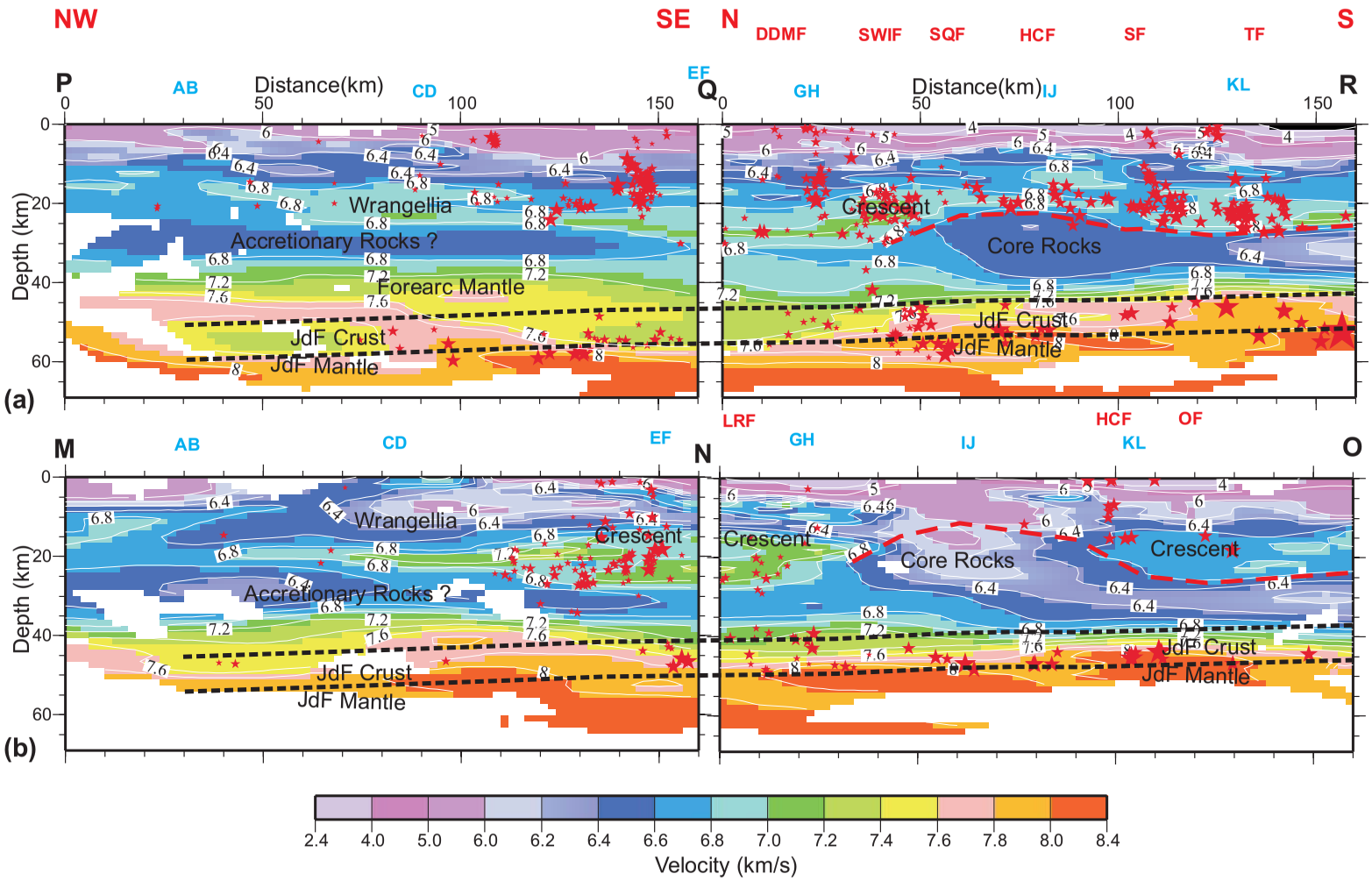
NW
SE
N
S
DDMF
SWIF
SQF
HCF
SF
TF
P
AB
Distance(km)
CD
EF
Q
GH
Distance(km)
IJ
KL
R
Depth (km)
Wrangellia
Accretionary Rocks ?
Forearc Mantle
JdF Crust
JdF Mantle
Crescent
Core Rocks
(a)
LRF
HCF
OF
M
AB
CD
EF
N
GH
IJ
KL
O
Wrangellia
Crescent
Accretionary Rocks ?
Core Rocks
JdF Crust
JdF Mantle
(b)
2.4
4.0
5.0
6.0
6.2
6.4
6.6
6.8
7.0
7.2
7.4
7.6
7.8
8.0
8.4
Velocity (km/s)

Figure 8

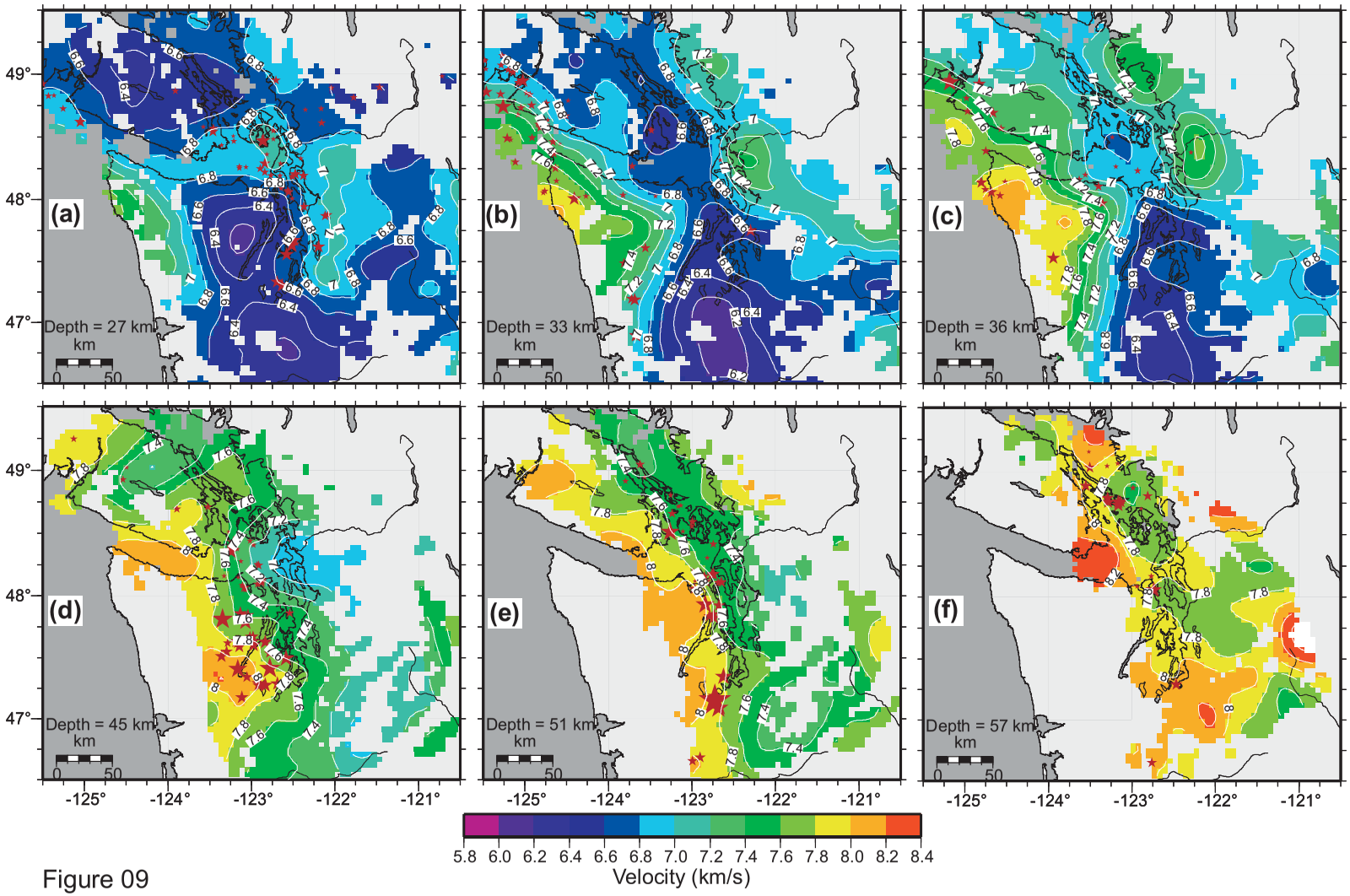
(a)
Depth = 27 km
(b)
Depth = 33 km
(c)
Depth = 36 km
(d)
Depth = 45 km
(e)
Depth = 51 km
(f)
Depth = 57 km
km
0 50
49°
48°
47°
-125°
-124°
-123°
-122°
-121°
5.8 6.0 6.2 6.4 6.6 6.8 7.0 7.2 7.4 7.6 7.8 8.0 8.2 8.4
Velocity (km/s)

Figure 09

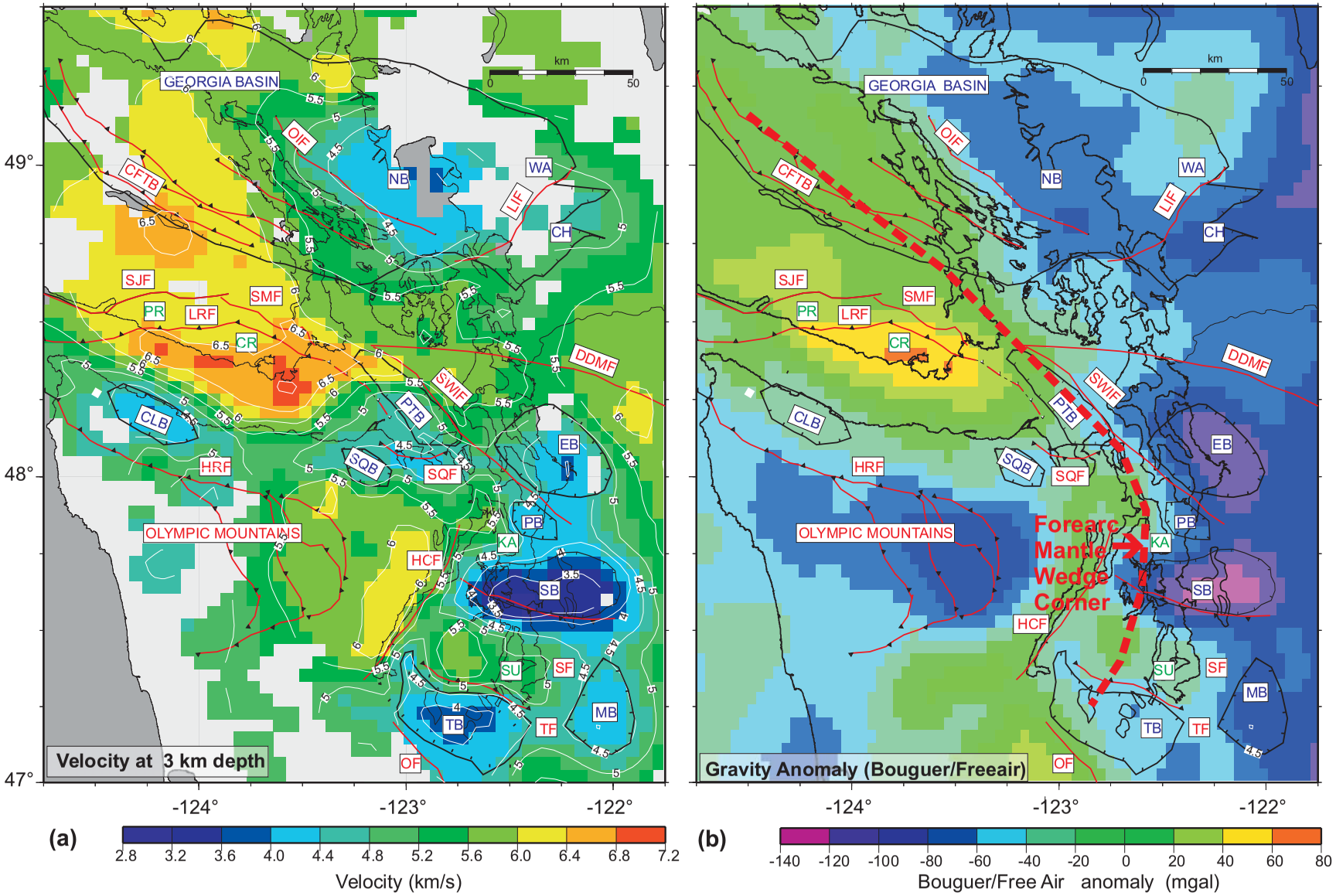
GEORGIA BASIN
OIF
CFTB
NB
WA
LIF
CH
SJF
SMF
PR
LRF
CR
DDMF
SWIF
PTB
CLB
EB
HRF
SQB
SQF
OLYMPIC MOUNTAINS
PB
KA
HCF
SB
SU
SF
MB
TB
TF
OF
Velocity at 3 km depth
Gravity Anomaly (Bouguer/Freeair)
Forearc Mantle Wedge Corner
km
0
50
49°
48°
47°
-124°
-123°
-122°
(a)
2.8 3.2 3.6 4.0 4.4 4.8 5.2 5.6 6.0 6.4 6.8 7.2
Velocity (km/s)
(b)
-140 -120 -100 -80 -60 -40 -20 0 20 40 60 80
Bouguer/Free Air anomaly (mgal)

Figure 10

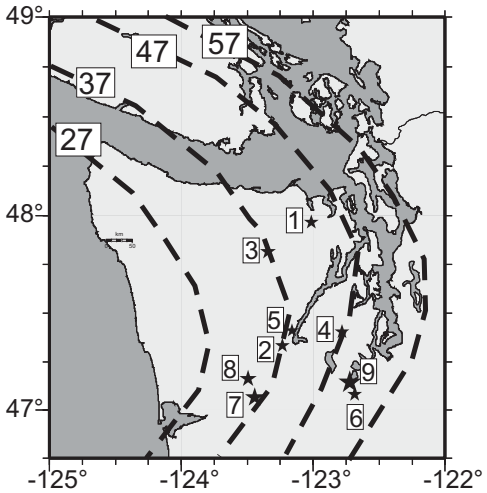

Figure 11